# Stratosphere–Troposphere Coupling and Links with Eurasian Land Surface Variability

JUDAH COHEN

*Atmospheric and Environmental Research, Inc., Lexington, Massachusetts*

MATHEW BARLOW

*University of Massachusetts—Lowell, Lowell, Massachusetts*

PAUL J. KUSHNER

*Department of Physics, University of Toronto, Toronto, Ontario, Canada*

KAZUYUKI SAITO

*Frontier Research Center for Global Change, Japan Agency for Marine-Earth Science and Technology, Yokohama, Kanagawa, Japan*

(Manuscript received 20 October 2006, in final form 30 January 2007)

ABSTRACT

A diagnostic of Northern Hemisphere winter extratropical stratosphere–troposphere interactions is presented to facilitate the study of stratosphere–troposphere coupling and to examine what might influence these interactions. The diagnostic is a multivariate EOF combining lower-stratospheric planetary wave activity flux in December with sea level pressure in January. This EOF analysis captures a strong linkage between the vertical component of lower-stratospheric wave activity over Eurasia and the subsequent development of hemisphere-wide surface circulation anomalies, which are strongly related to the Arctic Oscillation. Wintertime stratosphere–troposphere events picked out by this diagnostic often have a precursor in autumn: years with large October snow extent over Eurasia feature strong wintertime upward-propagating planetary wave pulses, a weaker wintertime polar vortex, and high geopotential heights in the wintertime polar troposphere. This provides further evidence for predictability of wintertime circulation based on autumnal snow extent over Eurasia. These results also raise the question of how the atmosphere will respond to a modified snow cover in a changing climate.

## 1. Introduction

In this report we examine the tropospheric precursors and horizontal structure of the multiple-week extratropical stratosphere–troposphere interaction events highlighted by Baldwin and Dunkerton (1999, 2001) and numerous follow-on studies (e.g., Cohen et al. 2002; Baldwin et al. 2003; Polvani and Waugh 2004; Limpasuvan et al. 2004, 2005; Reichler et al. 2005). These events consist of an annular-mode (Thompson and Wallace 2000) signature that starts in the stratosphere and progresses downward into the troposphere, where it persists for several weeks. The stratosphere–troposphere annular-mode events are always preceded by an anomalous lower-stratospheric planetary wave activity flux, but robust lower-tropospheric wave activity signatures of these events are more difficult to find (Polvani and Waugh 2004). This is because the troposphere is inherently more variable than the stratosphere and because the stratosphere is capable of generating downward-propagating annular-mode signals—i.e., stratospheric vacillations (e.g., Holton and Mass 1976; Plumb and Semeniuk 2003)—independently of the state of the troposphere.

The multiple-week time scale of extratropical stratosphere–troposphere interaction events suggests that stratospheric conditions could be used for long-range tropospheric forecasts (Baldwin et al. 2003; Charlton et al. 2003; Siegmund 2005). If robust tropospheric precursors to a significant portion of such events could be

*Corresponding author address:* Judah Cohen, AER, Inc., 131 Hartwell Ave., Lexington, MA 02421.
E-mail: jcohen@aer.com

DOI: 10.1175/2007JCLI1725.1

found, they might extend the practical forecasting range even further back in time. With this goal in mind, we here show, following the work of Cohen et al. (2002), that these extratropical stratosphere–troposphere interaction patterns can be partially predicted by conditions over the Eurasian land surface. In particular, we present a concise diagnostic of the stratosphere–troposphere interaction patterns in the Northern Hemisphere winter (sections 2 and 3) that focuses on the spatial patterns and demonstrates that the locus of lower-stratospheric wave activity occurs over Eurasia; we then show that these patterns are robustly linked to variations in snow cover over Eurasia in Northern Hemisphere autumn (section 4). It is clear that this link does not hold for all stratosphere–troposphere interaction events but does account for a significant portion of them. Besides long-range forecasts, our findings may have implications for understanding some relationships associated with the global warming trend; these are discussed in the conclusions.

## 2. Method

Our diagnostic of the stratosphere–troposphere interaction patterns described in the introduction combines information from two physically and temporally distinct fields. First, the December-mean vertical component of the Plumb (1985) wave activity flux (WAF) calculated from the NCEP–NCAR 40-Year Reanalysis (Kalnay et al. 1996) at 100 hPa for the Northern Hemisphere north of 20°N, for each year from 1948 to 2004, provides information about upward-propagating planetary waves. The vertical component of the WAF is given by

$$F = \Omega p \sin(2\phi) S^{-1} \{ v' T' - [2\Omega a \sin(2\phi)]^{-1} \partial(T'\Phi')/\partial\lambda \},$$

where $\Omega$ is the angular velocity of rotation, $p$ is pressure, $\phi$ is latitude, $v$ is meridional velocity, $T$ is temperature, $a$ is the mean radius of the earth, $\Phi$ is geopotential, $\lambda$ is longitude, and primes indicate the departure from the local climatological mean. The static stability $S = \langle -(p/H)\partial T/\partial p + \kappa T/H \rangle$, where angle brackets indicate the 20°–90°N polar-cap and climatological average, $\kappa = R/c_p$ and $H$ is the scale height. The field $F$ is useful for localizing in longitude and latitude the source of vertically propagating stationary planetary Rossby waves. The zonal mean of $F$ is proportional to the meridional eddy heat flux and the vertical component of the quasigeostrophic Eliassen–Palm flux.

The second field, the January-mean NCEP–NCAR Reanalysis sea level pressure (SLP) for the same domain for each year from 1949 to 2005, provides information about the lower-tropospheric circulation in the month following the December WAF anomaly. Both fields were each detrended, weighted by the square root of the cosine of the latitude, and normalized by the their respective mean standard deviation. Then, using both fields, a multivariate empirical orthogonal function (EOF) analysis was conducted to identify the primary patterns of common variability.

This approach is objective but heuristic: we look for modes that combine the December WAF and January SLP to create a diagnostic of those strong planetary wave events that culminate with a strong SLP signal in the troposphere. But what motivates our choice of months, that is, December for the WAF and January for the SLP? The characteristic time scale of stratosphere–troposphere interaction life cycles is several weeks, so we expect an offset between an initial wave-driving event and the subsequent circulation response. For example, Polvani and Waugh (2004) show that stratospheric geopotential height anomalies are correlated with the time-integrated lower-stratospheric WAF over the previous several weeks. To keep the analysis reproducible and applicable to the problem of seasonal forecasting (for which monthly anomaly forecasts are standard products), we choose to look at WAF in one calendar month and the circulation in the subsequent calendar month. January is a natural target month for looking at circulation anomalies for several reasons: it is the peak month for extratropical circulation variability, the month of strongest annular-mode coupling between the troposphere and stratosphere (Baldwin and Dunkerton 1999; Thompson and Wallace 2000), and a month of particular interest for seasonal forecasting. In section 3c, we discuss the sensitivity of our results to the choice of analysis time period.

We calculate the leading multivariate WAF/SLP EOF and its principal component time series, shown in Fig. 1. This EOF explains 15% of the combined variance in the two fields (maximum local WAF correlation is 0.8, maximum local SLP correlation is 0.74) and is well separated from the next EOF, which explains 7% of this variance. In the remainder of the article we refer to the principal component of the leading multivariate WAF/SLP EOF as the stratosphere–troposphere coupling index (STCI), or $s(t)$, where $t$ is a time index running from the 1948/49 to the 2004/05 December–January season. We discuss the characteristics of this mode in the next section.

A third physically distinct field we employ is a measure of October-mean snow cover extent over Eurasia, which is the surface forcing that we focus on in this study. This October-mean snow cover area index, which we call $a(t)$, merges a satellite-based dataset (Robinson et al. 1993) from 1967 to 2004 and Brown's

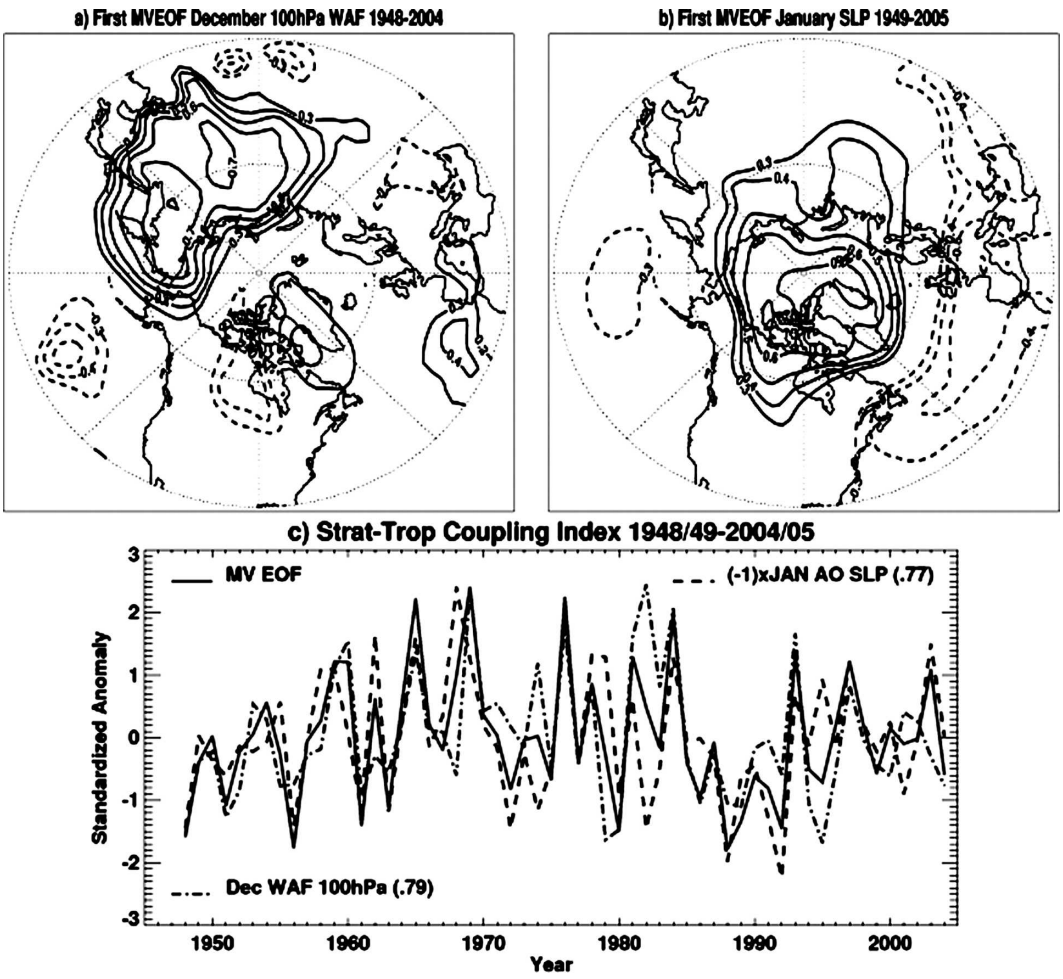


FIG. 1. (a) Correlation of the stratosphere–troposphere coupling index (STCI) with the vertical component of the December 100-hPa WAF. (b) Same as in (a), but for the correlation with January SLP. Contour interval for (a) and (b) is 0.1 starting with ±0.3. (c) The STCI (solid line) and the principal component time series for the first EOF of December 100-hPa vertical WAF (dashed line) and for the first EOF of the January SLP (dashed–dotted line; this is the negative of the January Arctic Oscillation index).

(2000) historical reconstruction, which is based on in situ observations, from 1948 to 1966. The standardized indices of $s(t)$ and $a(t)$ are shown in Table 1.

## 3. Results

### *a. A concise diagnostic of stratosphere–troposphere interactions*

In this section, we show that the multivariate EOF described in section 2 efficiently captures extratropical stratosphere–troposphere interaction events. First, we plot in Fig. 1 the WAF and SLP patterns that are associated with the STCI. Figure 1a shows the correlation of December 100-hPa WAF with $s(t)$, and Fig. 1b shows the correlation of January SLP with $s(t)$; covariance produces a similar pattern for both variables (not shown). The figure represents the positive phase of the multivariate EOF, chosen by convention. We see that the December WAF pattern in Fig. 1a has a strong positive center of action, corresponding to upward wave activity propagation, over a sector extending from eastern Europe to the east coast of Asia; this is also the region of greatest variance, climatologically. Furthermore, the center of greatest variability is over Siberia, highlighting the Eurasian sector as being particularly important for stratosphere–troposphere coupling.

The January SLP (Fig. 1b) signature strongly resembles the negative phase of the Arctic Oscillation (AO) or Northern Annular Mode (NAM), with centers of action over the Pacific, Atlantic, and Arctic (Thompson and Wallace 1998, 2000). The NAM itself corre-

TABLE 1. Detrended standardized STCI, which is the principal component of the multivariate EOF, and the Siberian October snow index as described in the text for the years 1948/49–2004/05.

| Year | STCI | Oct snow |
|---|---|---|
| 1948 | −1.59 | −1.11 |
| 1949 | −0.39 | −0.59 |
| 1950 | 0.03 | −0.94 |
| 1951 | −1.09 | −0.94 |
| 1952 | −0.23 | 1.20 |
| 1953 | 0.06 | 0.32 |
| 1954 | 0.57 | −1.16 |
| 1955 | −0.27 | −1.50 |
| 1956 | −1.77 | −0.44 |
| 1957 | −0.05 | −0.41 |
| 1958 | 0.27 | −0.27 |
| 1959 | 1.22 | 1.76 |
| 1960 | 1.21 | 2.04 |
| 1961 | −1.41 | 0.10 |
| 1962 | 0.63 | 0.88 |
| 1963 | −1.12 | −0.71 |
| 1964 | 0.59 | 0.37 |
| 1965 | 2.22 | 0.84 |
| 1966 | 0.21 | 0.56 |
| 1967 | −0.20 | −0.19 |
| 1968 | 0.98 | 1.13 |
| 1969 | 2.41 | 1.33 |
| 1970 | 0.36 | 1.52 |
| 1971 | 0.04 | 1.17 |
| 1972 | −0.83 | 1.12 |
| 1973 | −0.04 | 0.24 |
| 1974 | 0.03 | −0.07 |
| 1975 | −0.68 | −0.69 |
| 1976 | 2.25 | 3.45 |
| 1977 | −0.40 | 0.84 |
| 1978 | 0.87 | 0.23 |
| 1979 | −0.28 | −0.69 |
| 1980 | −1.50 | −1.10 |
| 1981 | 1.30 | −0.53 |
| 1982 | 0.48 | 0.53 |
| 1983 | −0.17 | −0.26 |
| 1984 | 1.99 | −0.13 |
| 1985 | −0.40 | −0.12 |
| 1986 | −0.96 | −0.48 |
| 1987 | −0.07 | −1.29 |
| 1988 | −1.78 | −1.90 |
| 1989 | −1.34 | −0.28 |
| 1990 | −0.62 | −1.00 |
| 1991 | −0.81 | −1.16 |
| 1992 | −1.45 | −0.58 |
| 1993 | 1.34 | 0.37 |
| 1994 | −0.50 | −1.10 |
| 1995 | −0.72 | 0.03 |
| 1996 | 0.22 | 0.20 |
| 1997 | 1.22 | −0.22 |
| 1998 | 0.23 | 1.00 |
| 1999 | −0.58 | 0.05 |
| 2000 | 0.15 | 0.34 |
| 2001 | −0.10 | 0.67 |
| 2002 | −0.02 | 1.85 |
| 2003 | 1.09 | 0.40 |
| 2004 | −0.59 | 0.66 |

sponds to the leading EOF of Northern Hemisphere extratropical January SLP, and we find that the correlation between the NAM index and the STCI is −0.77 (Fig. 1c). This implies, for example, that an anomalously negative NAM phase in January is strongly linked with an anomalously positive (upward) planetary WAF over Eurasia in December.

It is not surprising that the multivariate EOF is coherent with variations in December WAF and January SLP, since these fields are input to the EOF calculation. However, the fact that the multivariate EOF corresponds to high correlations with variability in both fields (maximum of 0.79 in WAF and 0.77 in SLP) strongly suggests that the two fields are coupled. In addition, we also find that the EOF captures the time-evolving signature of stratosphere–troposphere interaction events. In Fig. 2a, for example, we show the correlation between the STCI and the zonal mean WAF area averaged between 40° and 80°N as a function of height and calendar day, starting from 1 October. The index is coherent with the lower-stratospheric WAF in December, which is expected by construction. But beyond this, the figure shows that, for example, the positive phase of STCI is coherent with an upward WAF signature that extends from the lower troposphere to the stratosphere. In addition, there are moderate (correlations $<0.4$) but statistically significant precursors in the lower troposphere as early as October.

Figure 2b plots the correlation between the STCI and the polar cap (area averaged between 60° and 90°N) daily mean geopotential at each pressure level. As might be expected, the anomalous stratospheric wave-driving seen in Fig. 2a leads to a sign-consistent positive polar cap geopotential anomaly—for example, a positive anomaly in December WAF leads to anomalously high heights and a warmer polar stratosphere (not shown). This geopotential anomaly reaches into the troposphere in January, leading to the polar anticyclonic circulation anomaly seen in Fig. 1b. A more unexpected feature of this plot is the appearance of a positive height anomaly in the lower and midtroposphere in October and again in November; we return to these features below.

Looking at Figs. 1 and 2 together, we see that the multivariate EOF WAF/SLP mode exhibits a multiple-week life cycle characterized by a wave activity pulse originating over the Eurasian sector and a subsequent zonal-mean geopotential anomaly, whose sign is consistent with the WAF anomaly that propagates down into the lower troposphere. The multivariate EOF and its associated index $s(t)$ thus efficiently pick out those WAF events that lead to a subsequent tropospheric signal in midwinter.

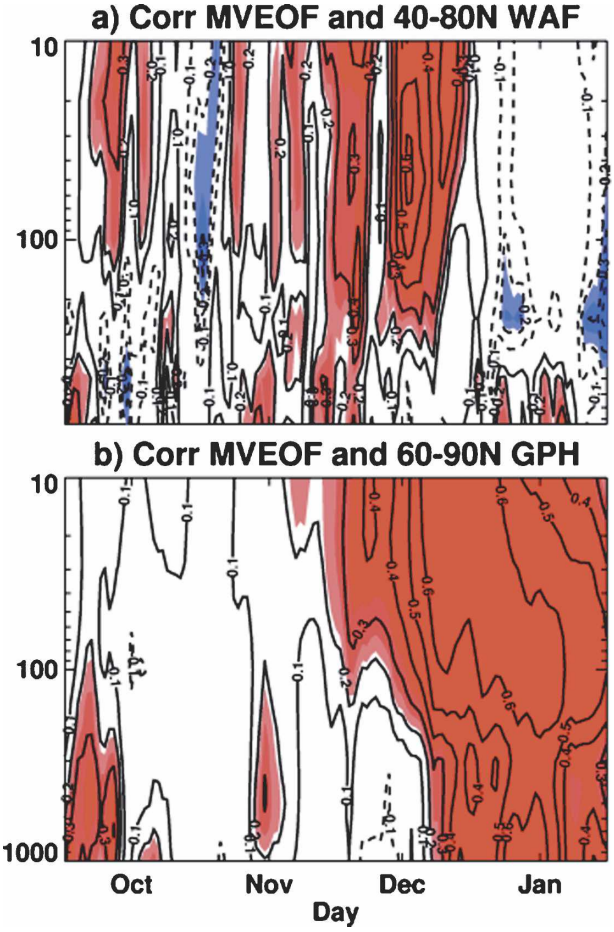


FIG. 2. Correlation of the principal component of multivariate EOF shown in Fig. 1 with (a) daily vertical wave activity flux averaged for all grid boxes between 40° and 80°N and all vertical levels between 850 and 10 hPa, and (b) daily geopotential height averaged for all grid boxes north of 60°N and all vertical levels between 1000 and 10 hPa. Those values exceeding 90%, 95%, and 99% confidence intervals based on Student's *t* test are denoted by light, dark, and darkest shading, respectively.

Why is the lower-stratospheric WAF EOF structure in Fig. 1a focused over the Eurasian sector? Since the climatological maximum in the vertical component of the Plumb flux is located there (Plumb 1985, his Fig. 4b) it might be expected that this region would also represent the area of maximum variability of this quantity, which the EOF would then identify. Plumb discusses how wave activity fluxes in this sector are forced by orography and diabatic heating, and presumably variations in these forcings contribute to the EOF pattern in Fig. 1a. In the next section, we discuss how one source of diabatic heating variability, related to Eurasian snow cover, might account for some portion of the WAF pattern in Fig. 1a and for the subsequent transient stratosphere–troposphere interactions.

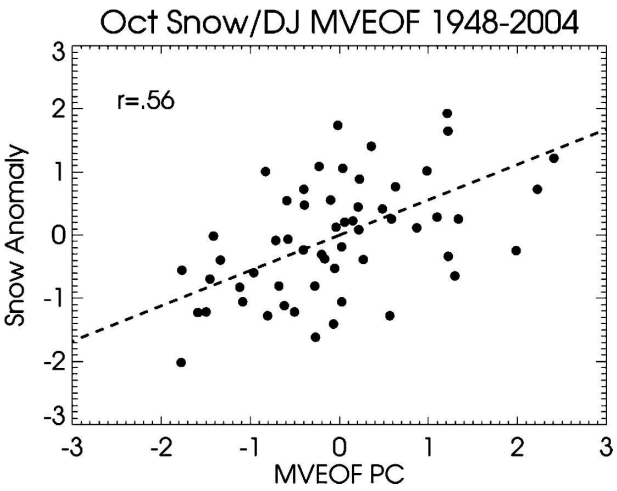


FIG. 3. Scatterplot of the principal component or time series associated with multivariate EOF shown in Fig. 1 and Eurasian October snow cover for the years 1948–2004. Correlation between the two time series is 0.56.

### b. October Eurasian snow

We now pursue the suggestion of Cohen and others that strong anomalies in October Eurasian snow cover can force a large-scale circulation response that involves a stratosphere–troposphere interaction event. The proposed mechanism is that high-albedo snow anomalies occurring sufficiently early in the fall can lead to a strong shortwave radiation anomaly at the surface and to a local diabatic-heating anomaly. The question then is whether this can excite a planetary Rossby wave response that sets off a stratosphere–troposphere interaction event. If the forcing is on a regional scale, the scale of the Rossby wave response would become independent of the scale of the forcing and reflect instead the detailed zonal mean-flow parameters as determined by the dynamics of planetary Rossby wave propagation [see, e.g., the stationary wave response to a narrow topographic ridge, discussed in Held et al. (2002)].

We find a good deal of statistical evidence to support the hypothesis that October Eurasian snow extent can predict stratosphere–troposphere interactions. First of all, the STCI, $s(t)$, and the October Eurasian snow index $a(t)$ are correlated at 0.56, which is statistically significant at the confidence limit greater than 99% based on the Student's *t* test. The scatterplot and associated linear fit of these two quantities are shown in Fig. 3. This associates a fraction of positive October snow events with an upward-propagating planetary wave pulse in December and a negative NAM response in the stratosphere and troposphere into January.

For further evidence of the predictive power of Eur-

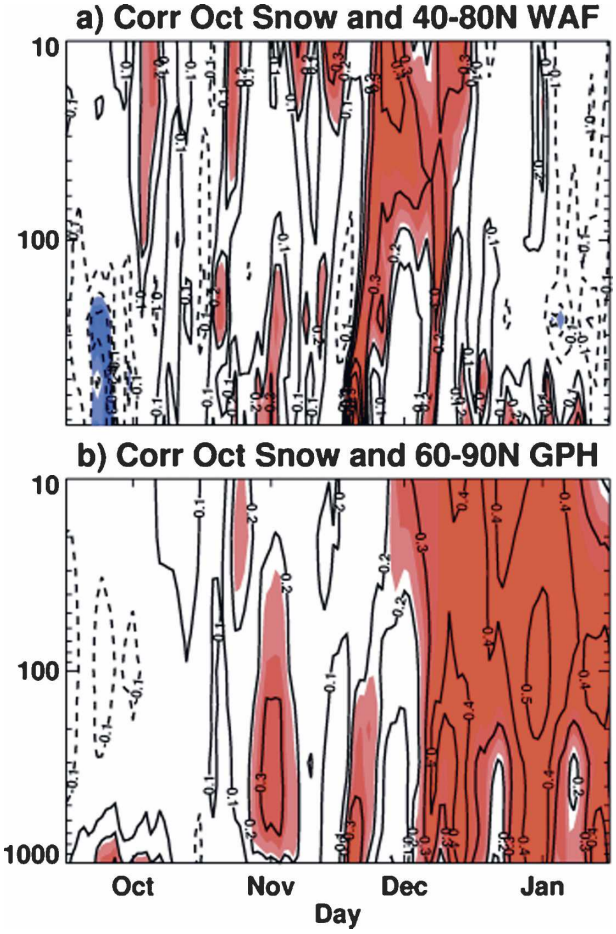


FIG. 4. Correlation of the areal extent of October Eurasian snow cover with (a) daily vertical wave activity flux averaged for all grid boxes between 40° and 80°N and all vertical levels between 850 and 10 hPa, and (b) daily geopotential height averaged for all grid boxes north of 60°N and all vertical levels between 1000 and 10 hPa. Those values exceeding 90%, 95%, and 99% confidence intervals based on Student's *t* test are denoted by light, dark, and darkest shading, respectively.

asian snow cover, we look to the time-evolving signature of the WAF and of the circulation that is coherent with the snow index $a(t)$. Figure 4a plots the day-by-day correlation of the October snow index $a(t)$ with the areal-mean WAF, and Fig. 4b plots the correlation of $a(t)$ with the polar cap mean geopotential height. That is, Fig. 4 is the same as Fig. 2, except that October snow cover area is substituted for the STCI. We see here that the October snow index is coherent with planetary wave pulses that originate in the troposphere in November and with a strong pulse that propagates from the lower troposphere into the stratosphere in December. Furthermore, we see a similar pattern in the geopotential correlations in Fig. 4b to what was seen in Fig. 2b; the resemblance and the fact that a vertically coherent correlation between October snow and the extratropical circulation emerges in December and survives into January is remarkable.

In Fig. 4 we see that the correlations between October snow cover and the atmospheric circulation are not greatest during October but almost 3 months later, in January. This suggests that the high correlations between snow cover and winter climate are not simply due to atmospheric conditions in October and that snow cover does not act simply as a reservoir of atmospheric memory. Figures 2 and 4 suggest that a series of relatively weak WAF pulses act to precondition the stratosphere prior to the main pulse. We cannot explain the timing of the individual WAF pulses through the fall–winter season but expect that these pulses are tied to the positive NH tropospheric polar cap height anomalies in fall seen in Figs. 2 and 4. This connection is suggested by previous work of Cohen and others (see Cohen et al. 2001, 2002) that links positive lower-tropospheric geopotential height anomalies over Eurasia in fall to negative NAM events in the troposphere in winter.

### c. *Sensitivity of results to analysis time period*

The restricted December/January analysis period, and the fact that we have retained only the leading mode of the multivariate EOF, means that our STCI cannot capture all the stratosphere–troposphere coupling events. In particular, the North Atlantic sector represents another source region for vertical WAF from the troposphere into the stratosphere (Plumb 1985), and not all STC events will result in NAM circulation signatures, and many STC events occur outside the December/January time period (Baldwin and Dunkerton 1999; Thompson and Wallace 2000).

In this subsection, we focus on how sensitive our results might be to a change of analysis time period. We proceed as follows:

1) We compute the first EOF of the vertical component of the WAF at 100 hPa for the months using a time series of monthly averaged WAF as a function of latitude and longitude from 40° to 80°N, including the autumn-to-winter months (September–January) only. The leading mode, shown in Fig. 5a, closely resembles the pattern shown in Fig. 1a, with the main center of variability over northern Eurasia.
2) We then repeat step 1 but for the SLP as a function of latitude and longitude from 20° to 90°N, in a time period lagged by 1 month from the WAF, that is, for the months October–February. The leading mode, shown in Fig. 5b, appears as a classical AO pattern, as in Fig. 1b.

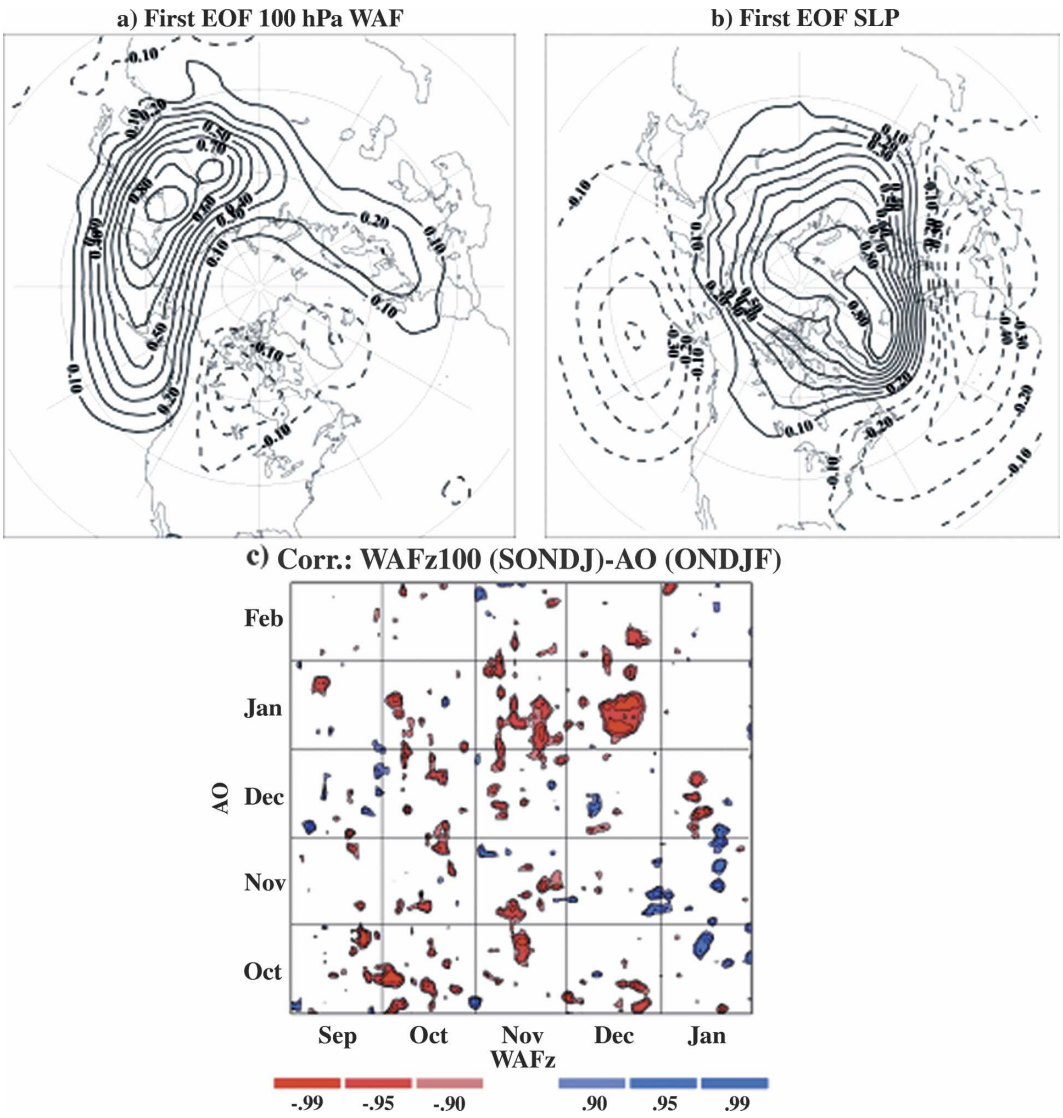


FIG. 5. (a) The first EOF of 100-hPa vertical wave activity flux for the 5-month period September–January shown as a correlation between the principal component and the WAF. (b) The first EOF of SLP for the 5-month period October–February shown as a correlation between the principal component and the SLP. Contour interval for (a) and (b) is 0.1 starting with ±0.1. (c) Daily lead-lag correlations for the two EOFs shown in (a) and (b) projected on to the daily data.

3) We form *daily* time series indices for the patterns in Figs. 5a and 5b by calculating the projection of these patterns onto the daily WAF and SLP, using 1 September–31 January for the WAF and 1 October–28 February for the SLP. We plot the lagged temporal correlation between these two time series in Fig. 5c; only statistically significant points are shaded, and lines have been drawn to delineate the months.

In Fig. 5c, the greatest percentage of statistically significant correlations occurs between December WAF and January SLP. This further supports our choice of time period, and the similarity between Figs. 5a,b and Figs. 1a,b emphasizes the overall robustness of the coupled mode of variability we have identified. Interestingly, snow cover could be thought of as an independent variable corroborating these results. As seen from Fig. 4, correlations between October snow cover and WAF are highest in December, and those between October snow cover and geopotential heights are highest in January.

The region with the second greatest percentage of statistically significant correlations in Fig. 5c is that of November WAF and January SLP. This is consistent

with Fig. 2a and with the results of Polvani and Waugh (2004), who found that the dominant mode of geopotential height variability in the stratosphere was highly correlated with the vertical WAF at 100 hPa from the prior 6 weeks. So if a NAM event originates in the stratosphere and propagates down to the surface in January, upward WAF would contribute to the event not only from December but from November as well.

Because of the patchiness of the significance regions in Fig. 5c, we assess, using a Monte Carlo test, whether the locally statistically significant regions identified by the *t* test were indeed robust. In this test, we generate 1000 random time series with the same autocorrelation statistics as the WAF and AO time series and compute the percent area of the lag correlation found to be statistically significant above the 95% threshold. This analysis shows that only the statistically significant region of correlations between the December WAF and January AO is robust. Thus, although the results presented in Fig. 5c suggest a more extended period of stratosphere–troposphere coupling throughout the fall and winter months, our limited analysis highlights December and January as the preferred months for upward WAF and the resulting tropospheric AO anomaly.

## 4. Conclusions

To summarize our findings, we have developed a concise diagnostic of stratosphere–troposphere interactions that captures those strong lower-stratospheric planetary wave activity events that later connect to the surface. The locus of the lower-stratospheric wave activity is over Eurasia with the center over Siberia, collocated with the climatological maximum of variance. Also, the resultant atmospheric response at the surface is closely related to the AO or NAM pattern of variability. We further show that this type or mode of coupling is favored in the December to January time frame.

We have found that the STCI arising from this analysis is coherent with October Eurasian snow extent, which reveals a connection between October Eurasian snow cover and stratosphere–troposphere interaction events. Typical correlations, shown in Fig. 4, are moderate ($<0.5$) but significant, suggesting that a significant portion of the anomalous snow events in October are tied to stratosphere–troposphere circulation anomalies more than 8 weeks later. The observational results presented here linking variability in snow cover with stratosphere–troposphere coupling are consistent with the modeling results of Gong et al. (2002). This study showed that interannual variations in snow cover are required to capture the observed significant correlations between the tropospheric NAM and the stratospheric NAM.

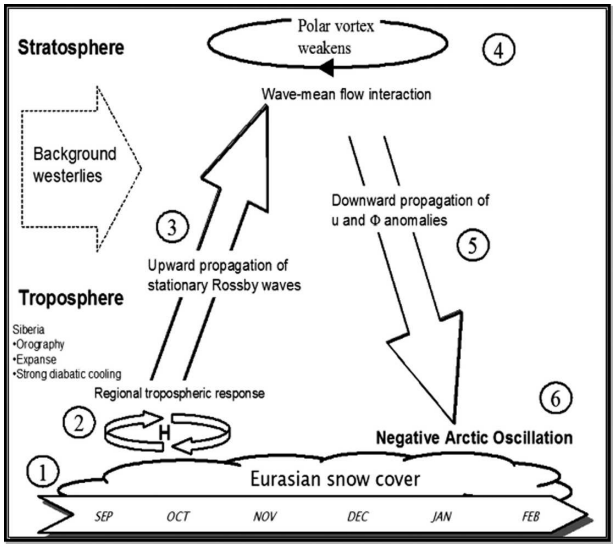


FIG. 6. Conceptual model for how fall snow cover modifies winter circulation in both the stratosphere and the troposphere; case for extensive snow cover illustrated: 1) Snow cover increases rapidly in the fall across Siberia, when snow cover is above normal. 2) Diabatic cooling helps strengthen the Siberian high and leads to below normal temperatures. 3) Snow-forced diabatic cooling in proximity to the high topography of Asia increases upward flux of wave activity from the troposphere, which is absorbed in the stratosphere. 4) Strong convergence of WAF leads to higher geopotential heights, a weakened polar vortex, and warmer temperatures in the stratosphere. 5) Zonal mean geopotential height and wind anomalies propagate down from the stratosphere into the troposphere all the way to the surface. 6) Dynamic pathway culminates with strong negative phase of the Arctic Oscillation at the surface.

We outline in Fig. 6 (based on Saito 2003; see also Reichler et al. 2005, their Fig. 1) a conceptual model of the dynamical pathway demonstrated by the statistically significant relationship among all the variables discussed above. October is the month snow cover makes its greatest advance, mostly across Siberia. October is also the month in which the Siberian high, one of the three dominant centers of action across the NH, forms. In years when snow cover is above normal this leads to a strengthened Siberian high and colder surface temperatures across Northern Eurasia in the fall. We suggest that the intensification of the Siberian high, along with the thermal impacts of enhanced snow cover and topographic forcing, corresponds to a positive wave activity flux anomaly in the late fall and early winter, leading to stratospheric warming and to the January tropospheric negative AO response we have described.

There are important implications of this work for seasonal forecasting. We have described here a statis-

tically significant relationship between time-leading extratropical boundary condition anomalies and time-lagging extratropical circulation anomalies. Furthermore, we have provided a diagnostic that can be used as an aid in operational monthly to seasonal forecasts. This complements ENSO-based predictors and suggests that there is hope for improving seasonal forecasts from extratropical indicators. Indeed, winter forecasts that incorporate snow cover as one of its predictors have demonstrated greater skill than forecasts that rely exclusively on ENSO (Cohen and Fletcher 2007).

We are also exploring the implications of this work for longer-term climate trends. If fall snow extent forces a consistent NAM response in winter, through the combination of diabatic and planetary wave generation mechanisms as we have described, then we expect that long-term trends in snow extent will be linked to long-term NAM variability and trends. Initial work along these lines (Cohen and Barlow 2005) demonstrates that there are in fact statistical connections between long-term trends in Eurasian snow cover and the tropospheric circulation. We are currently building on the Cohen–Barlow results with a focus on the stratosphere–troposphere interactions we have discussed here.

*Acknowledgments.* Cohen was supported by NSF Grant 0443512, Barlow by NSF Grant 0603555, and Kushner by the Canadian Foundation for Climate and the Atmospheric Sciences. We thank the efforts of two reviewers whose comments improved the quality of the original manuscript.

## REFERENCES

Baldwin, M. P., and T. J. Dunkerton, 1999: Propagation of the Arctic Oscillation from the stratosphere to the troposphere. *J. Geophys. Res.,* **104,** 30 937–30 946.

——, and ——, 2001: Stratospheric harbingers of anomalous weather regimes. *Science,* **294,** 581–584.

——, D. B. Stephenson, D. W. J. Thompson, T. J. Dunkerton, A. J. Charlton, and A. O'Neill, 2003: Stratospheric memory and extended-range weather forecasts. *Science,* **301,** 636–640.

Brown, R. D., 2000: Northern Hemisphere snow cover variability and change, 1915–97. *J. Climate,* **13,** 2339–2355.

Charlton, A. J., A. O'Neill, D. B. Stephenson, W. A. Lahoz, and M. P. Baldwin, 2003: Can knowledge of the state of the stratosphere be used to improve statistical forecasts of the troposphere? *Quart. J. Roy. Meteor. Soc.,* **129,** 3205–3224.

Cohen, J., and M. Barlow, 2005: The NAO, the AO, and global warming: How closely related? *J. Climate,* **18,** 4498–4513.

——, and C. Fletcher, 2007: Improved skill of Northern Hemisphere winter surface temperature predictions based on land–atmosphere fall anomalies. *J. Climate,* **20,** 4118–4132.

——, K. Saito, and D. Entekhabi, 2001: The role of the Siberian high in Northern Hemisphere climate variability. *Geophys. Res. Lett.,* **28,** 299–302.

——, D. Salstein, and K. Saito, 2002: A dynamical framework to understand and predict the major Northern Hemisphere mode. *Geophys. Res. Lett.,* **29,** 1412, doi:10.1029/2001GL014117.

Gong, G., D. Entekhabi, and J. Cohen, 2002: A large-ensemble model study of the wintertime AO–NAO and the role of interannual snow perturbations. *J. Climate,* **15,** 3488–3499.

Held, I. M., M. Ting, and H. Wang, 2002: Northern winter stationary waves: Theory and modeling. *J. Climate,* **15,** 2125–2144.

Holton, J. R., and C. Mass, 1976: Stratospheric vacillation cycles. *J. Atmos. Sci.,* **33,** 2218–2225.

Kalnay, E., and Coauthors, 1996: The NCEP/NCAR 40-Year Reanalysis Project. *Bull. Amer. Meteor. Soc.,* **77,** 437–471.

Limpasuvan, V., D. W. J. Thompson, and D. L. Hartmann, 2004: The life cycle of Northern Hemisphere sudden stratospheric warmings. *J. Climate,* **17,** 2584–2596.

——, D. L. Hartmann, D. W. J. Thompson, K. Jeev, and Y. L. Yung, 2005: Stratosphere-troposphere evolution during polar vortex intensification. *J. Geophys. Res.,* **110,** D24101, doi:10.1029/2005JD006302.

Plumb, R. A., 1985: On the three-dimensional propagation of stationary waves. *J. Atmos. Sci.,* **42,** 217–229.

——, and K. Semeniuk, 2003: Downward migration of extratropical zonal wind anomalies. *J. Geophys. Res.,* **108,** 4223, doi:10.1029/2002JD002773.

Polvani, L. M., and D. W. Waugh, 2004: Upward wave activity flux as a precursor to extreme stratospheric events and subsequent anomalous surface weather regimes. *J. Climate,* **17,** 3548–3554.

Reichler, T., P. J. Kushner, and L. M. Polvani, 2005: The coupled stratosphere–troposphere response to impulsive forcing from the troposphere. *J. Atmos. Sci.,* **62,** 3337–3352.

Robinson, D. A., K. F. Dewey, and R. R. Heim Jr., 1993: Global snow cover monitoring: An update. *Bull. Amer. Meteor. Soc.,* **74,** 1689–1696.

Saito, K., 2003: Seasonal to sub-decadal climatic covariability of snow cover and atmosphere in the Northern Hemisphere. Ph.D. thesis, Nagoya University, 161 pp.

Siegmund, P., 2005: Stratospheric polar cap mean height and temperature as extended-range weather predictors. *Mon. Wea. Rev.,* **133,** 2436–2448.

Thompson, D. W. J., and J. M. Wallace, 1998: The Arctic Oscillation signature in the wintertime geopotential height and temperature fields. *Geophys. Res. Lett.,* **25,** 1297–1300.

——, and ——, 2000: Annular modes in the extratropical circulation. Part I: Month-to-month variability. *J. Climate,* **13,** 1000–1016.